TDP-43 pathology is linked to motor neuron loss but is independent of stress granules *in vivo*

Alicia Dubinski[1,3], Ala Ferdi[1,3†], Mariam Choughari[1,3†], Holly Spence[4], Arpita Adhikary[2,3], Carolane Fauchon[2,3], Melissa Touati[3], Myriam Gagné[2,3], Martha Liu[3], Sarah Peyrard[3], Jenna Gregory[4,5], Christine Vande Velde[1-3]

[†]These authors contributed equally to this work.

Abstract

Nuclear depletion and cytoplasmic aggregation of TDP-43 are pathological hallmarks of several neurodegenerative diseases, including amyotrophic lateral sclerosis (ALS), frontotemporal dementia (FTD), Alzheimer's disease, and the recently defined limbic-predominant age-related TDP-43 encephalopathy (LATE). Chronic activation of the integrated stress response (ISR) and persistence of stress granules, phase-separated assemblies proposed to function as a protective mechanism, have been hypothesized to initiate the formation of pathological TDP-43 inclusions observed in post-mortem neurons. However, recent clinical trials targeting the ISR and stress granule dissolution failed to demonstrate clinical benefit despite robust target engagement, calling this model into question. Here, we employ a recurrent hyperthermia paradigm to directly examine the relationship between stress granules and TDP-43 pathology *in vivo*. We find that RNA-binding proteins classically associated with stress granules persist as phase-separated cytoplasmic structures in spinal motor neurons of both non-transgenic and mutant TDP-43 mice. Importantly, these structures are reversible and spatially distinct from TDP-43 puncta. Moreover, in a mutant TDP-43 mouse model with an impaired acute stress granule response, stress exposure induces TDP-43 nuclear export and cytoplasmic accumulation. Recurrent stress in these mice leads to a selective loss of spinal α-motor neurons. Together, our findings demonstrate that TDP-43 nuclear clearance and cytoplasmic demixing occur independently of stress granules *in vivo*, challenging prevailing models of TDP-43 pathogenesis and highlighting important implications for therapeutic strategies targeting the ISR.

Author affiliations:

1. Department of Neuroscience, Université de Montréal, Montréal, Québec, H3C 3J7, Canada

2. Department of Biochemistry, Université de Montréal, Montréal, Québec, H3C 3J7, Canada

3. Centre de Recherche du Centre Hospitalier de l'Université de Montréal (CRCHUM), Montréal, Québec, H2X 0A9, Canada

4. Institute of Medical Sciences, University of Aberdeen, Aberdeen, AB25 2ZD, UK

5. Department of Pathology, NHS Grampian Tissue Biorepository, Aberdeen, AB25 2ZD, UK

Correspondence to: **Christine Vande Velde, Ph.D.**

Department of Neurosciences, Université de Montréal

CRCHUM-Tour Viger

900, rue Saint-Denis, R09.474

Montreal, QC, CANADA H2X 0A9

Email: c.vande.velde@umontreal.ca

Running title: TDP-43 pathology without stress granules

Keywords: Amyotrophic lateral sclerosis, stress granules, TDP-43, neurodegeneration, motor neurons, Tia1

Abbreviations: No abbreviations list.

Introduction

There is an immediate need in the field to validate whether targeting the stress granule pathway is a valid therapeutic strategy for ALS/FTD and other neurodegenerative diseases. Stress granules form as part of the integrated stress response (ISR) and are proposed to act as triage sites for polyadenylated (polyA) mRNA as well as signaling hubs for pathways such as apoptosis[1,2]. Importantly, they are transient cytoplasmic structures that form via liquid-liquid

phase separation during external insults, and disassemble rapidly following abatement of the stress exposure[3]. In ALS, chronic upregulation of the ISR has been observed in both patient samples and animal models[4,5], and RNA binding proteins (RBPs) classically catalogued as stress granule proteins, such as TIA-1 and HuR, have been reported to co-label cytoplasmic TDP-43 aggregates in post-mortem tissues[6,7]. Due to a plethora of data primarily derived from *in vitro* overexpression systems, a prevailing hypothesis in the field is that persistent stress granules, caused by failed stress granule disassembly, act as seeds that precede TDP-43 aggregates and are neurotoxic[8–10]. Moreover, recent work has suggested that modulating stress granule dynamics with the small molecule lipoamide can reduce the axonal damage observed in mutant FUS expressing iPSC-derived motor neurons as well as improve behavioral phenotypes in mutant TDP-43 and FUS *Drosophila* models[11]. Recent clinical efforts to dampen the ISR using eIF2B agonists (DNL-343 & Fosigotifator), and thus abolish persistent stress granules, failed to show clinical improvements in ALS patients, despite clear target engagement for DNL-343[12,13]. More recently, the protective nature of stress granules has been investigated. For example, stress granules serve a protective role in fly models of ALS and FTD, as their dysfunction is associated with more severe disease outcomes[14,15]. In addition, in a mouse model expressing near-physiological levels of the ALS-linked TDP-43 mutation M337V, stress granule assembly is defective in motor neurons *in vivo* and is not correlated to TDP-43 translocation events[16]. It remains unknown whether stress granule dysfunction (protective or toxic) is linked to ALS pathogenesis.

It has been proposed that ALS onset is a combination of genetic predisposition, aging, and environmental insults[17]. While many transgenic mouse models that have been generated via TDP-43 overexpression (accumulating >2-fold over the endogenous) show clear motor phenotypes and neurodegeneration, knock-in models tend to show very mild and late-onset behavioral phenotypes, many of which are more closely associated with FTD[18–21]. While the field has been dominated by studies demonstrating a gain of toxicity owing to TDP-43 cytoplasmic aggregation, there has a recent shift towards a TDP-43 loss-of-function (LOF) hypothesis. Specifically, the loss of TDP-43 mediated repression of cryptic exons, such as those found in *STMN2* and *UNC13A*, which correlates positively with TDP-43 pathology in patients[22–26].

There is a clear need for improved TDP-43 mouse models that can advance our understanding of the relationship between TDP-43 LOF, TDP-43 aggregation, and disease pathogenesis[19,27]. One way to accomplish this is by challenging existing TDP-43 models with

an environmental insult ("two hit" models) to induce more severe molecular and behavioral phenotypes. Along this line, a recent study has shown that challenging a mouse model expressing the ALS-associated *C9orf72* repeat expansion with repetitive traumatic brain injury (TBI) leads to TDP-43 translocation, reduced neuron density, and worsened behavioral phenotypes[28]. Developing "two hit" models that incorporate genetic predisposition and environmental insult, rather than models that utilize supraphysiological expression of TDP-43, is anticipated to improve translation of future therapeutics.

In this study, we adapted our previously published acute hyperthermia model to determine if stress granules could persist *in vivo* and whether this associated with TDP-43 pathology or motor neuron death. In addition, we aimed to evaluate how this environmental stress influenced TDP-43 translocation and aggregation in TDP-43^{M337V} mice, which display defective stress granule assembly and increased TDP-43 nuclear clearance during acute hyperthermia. Our data demonstrate that stress granule proteins, but not cytoplasmic demixed polyadenylated mRNA, persist in the motor neurons of mice exposed to whole body recurrent hyperthermia, but this is reversible and not associated with neuronal survival. Our data also indicate that cytoplasmic TDP-43 foci are spatially independent of these structures. Lastly, we show that recurrent heat stress exposures in this TDP-43 mouse model induces TDP-43 nuclear clearance, accumulation of cytoplasmic TDP-43 puncta, and selective death of alpha motor neurons.

Materials and methods

Animals

The use of animals and all procedures were performed in according to guidelines of the Canadian Council on Animal Care and were approved by the CRCHUM animal care committee (CIPA). Mouse lines used were TDP-43^{M337V} BAC transgenic mice[29], *Tardbp*^{Q331K} knock-in mice[20], and NEFH::rNLS8 mice[30]. For acute hyperthermia experiments, only males were used for *Tardbp*^{Q331K} (4M) and both males and females were used for rNLS8 (2 weeks off dox). Only males were used for all recurrent hyperthermia experiments in the manuscript, as they are reported to have a stronger phenotype in the TDP-43^{M337V} mouse line[29]. For data with non-transgenic mice, all mice were littermates with no transgene expression in the TDP-

43^{M337V} colony. Mice used in Figure 1 were a combination of B6/N mice (Charles River) and NTg littermates from TDP-43^{M337V} mice.

Acute hyperthermia treatment

Acute hyperthermia was performed as previously described[16]. Briefly, Mice were anesthetized by intra-peritoneal (IP) injection of anesthetic cocktail (0.15cc/10g) (1mg/ml ketamine, 0.5 mg/ml xylazine and 0.1mg/ml acepromazine) and were put under 4% isofluorane until loss of reflex. Initial internal temperature was measured immediately (PhysioSuite, Kent Scientific). Mice were then placed in a 44°C incubator supplemented with 1L/min of oxygen. Heart rate and oxygen saturation were monitored during the 20 mins acute stress using MouseOx® (Starr Life Sciences, USA). After stress, the final internal temperature was measured before sacrifice. Mice were perfused with 4% PFA and processed for imaging or tissues were collected and flash frozen in liquid N_2 for biochemical analyses.

Recurrent hyperthermia treatment

For the 60 mins hyperthermia treatment, awake mice were weighed and starting core temperatures were taken immediately (PhysioSuite, Kent Scientific). Mice were placed in a restraining device (Stoelting) and lowered into their cage. Cages were placed into an incubator set to 40˚C supplemented with 1L/min O_2 and a 60 min timer was started. Mice were observed every 10 mins to ensure they were adequately moving and not in distress. After 60 mins of hyperthermia, mice were removed from restrainers, and the internal body temperature was taken immediately. Mice were then given free access to wet food and water for the 15 min rest period. This was repeated immediately a for a second 60 min stress. After the second 15 min rest period (total of 150 mins), mice were given 1.0 mL of saline for hydration in addition to diet-gel and wet food to prevent weight loss. The 150 min hyperthermia paradigm was repeated twice per week for 4 weeks. The next day, mice were sacrificed by perfusion with 4% PFA or for tissue collection by flash freezing in liquid N_2. Tissues were subsequently cryopreserved, embedded in OCT, and sectioned. Mice in the recovery paradigm (12M + 1M hyperthermia + 4M recovery) were monitored biweekly throughout the recovery period. Following this, they were sacrificed by perfusion with 4% PFA and processed. Mice were weighed three times per week throughout the hyperthermia and biweekly for the recovery period.

Immunofluorescence & Fluorescence in situ hybridization (FISH)

Floating sections of lumbar spinal cords (L3-L5, 30μm) were used for staining. For all labellings, sections were washed in Sorenson's PBS (13mM NaH_2PO_4, 87mM Na_2HPO_4, pH 7.6) then blocked with 3% BSA followed by incubation of primary antibodies (TDP-43 Proteintech 10782-2-AP; 1/200, TDP-43 R&D Systems MAB7778; 1/200, TiaR BD Biosciences 610352; 1/100, HuR SantaCruz sc-5261; 1/300, G3BP2 Cedarlane A302-040A; 1/100, TDP-43 S409/410 Cedarlane 829901; 1/200, p62 Sigma P0067; 1/100), human-specific TDP-43 #60019-2-Ig; 1:10,000) overnight at 4°C. The following day, spinal cords were washed and incubated with fluorescently conjugated secondary antibodies (1/200) to the desired species, stained with Hoescht, and mounted on slides with ProLong Antifade reagent (Invitrogen). For fluorescence in situ hybridization, sections were washed in 5X SSC buffer, acetylated with acetic anhydride (3μL/mL), permeabilized with Triton-X-100 (0.5% in 5X SSC), then incubated in hybridization buffer (0.1M TEA pH8, 25% formamide, 1mg/mL yeast RNA, 0.01% BSA, 10% dextran sulfate) for 2 hr at 37°C. The oligo-dT probe (1.3ng/μL, Texas Red) was diluted in hybridization buffer then added to spinal cords for incubation overnight at 37°C. The following day, spinal cords were diluted and washed in 5X SSC buffer, stained with Hoescht, and mounted with ProLong Antifade reagent (Invitrogen). Images were acquired with a 63X oil (1.7 NA) objective on a confocal microscope (SP5; Leica) using LAS-X software (Leica).

Labelling with TDP-43APT

Coronal sections (8 μm) were mounted onto adhesive slides, fixed with 4% PFA for 1 hr and washed in PBS-T (0.05% Tween) for 10 mins. Biotin blocking was carried out using a kit (Abcam, ab64212) as per the manufacturer's guidelines followed by washing in PBST (0.01% Tween). A protein block was performed using the Novolink Polymer detection system (Leica Biosystems, Newcastle, UK). TDP-43 aptamer (1/100, TDP-43^{Apt} CGGUGUUGCU with a 3' Biotin-TEG modification, ATDBio, Southampton, UK) prepared in protein block was applied to the tissue and incubated for 3 h at 4 °C followed by incubation with 4% PFA overnight at 4 °C. Sections were incubated with primary and secondary antibodies (1/100 goat-anti biotin Ab6652, 1/200 A647 donkey anti-goat Ab150135) then washed and mounted with Vectashield medium with DAPI (Vector labs, H-

1200). Images were acquired with a ZEISS AxioScan Z1 slide scanner at 20X magnification microscope at 20X magnification.

Motor neuron counting

Motor neuron counting was done using immunofluorescence on lumbar spinal cords (L3-L5). The same immunofluorescence protocol was followed using ChAT (Millipore AB144P; 1/100) and NeuN (Thermo Fisher PA5-78499; 1/500) primary antibodies. Between 7-10 sections, at least 150 μm apart, were imaged per mouse. Alpha motor neurons were stained for both ChAT and NeuN, while gamma motor neurons were stained positive for ChAT but do not have a NeuN signal [31]. Images were acquired with a 20X (1.25 NA) objective and analyzed using Cell Counter on ImageJ.

Image analysis

Cells were scored as positive for stress granules if they displayed at minimum 2 puncta that measured at least 0.15 μm^2. A minimum of 15 motor neurons were analyzed per mouse. Cells with TiaR or TDP-43 nuclear depletion were counted manually. Images were taken in lumbar spinal cords focused on the ventral horn, and a cell was counted if it had a nuclear size of at least 20μm^2. For TiaR puncta, cells were scored as positive if they displayed a minimum of 5 puncta measuring at least 0.15 μm^2. For TDP-43 puncta, cells were considered positive if they had a minimum of 5 puncta measuring 0.15 μm^2, or a single punctum that was a minimum of 1 μm^2, due to the background of the antibody staining. All image analysis was done using ImageJ.

Granularity index was calculated in MatLab using the Sobel operator for edge detection[16]. Edges were detected in 2-3 cytosolic sections per cell and then divided by the size of each section to give the granularity index with unit edges/pixel. Granularity is then normalized to control for each genotype.

Cell culture

Mouse neuroblastoma cells (N2A, gift from Nicole Leclerc) were maintained in DMEM at 37C and 5% CO2. For siRNA transfection, non-targeting and TDP-43 targeting siRNAs (Dharmacon #D-001810-10-20, #L-040078-01-0020) were transfected using oligofectamine

for 5 hours (Invitrogen 12252-011) and collected for RNA and protein extraction 72 hours later.

RT-PCR

Total RNA was extracted from cell pellets (N2A) using QIAGEN RNeasy mini kit according to the manufacturer instructions. RNA was isolated from mouse spinal cords using trizol/chloroform followed by isopropanol preceiptation. Residual genomic DNA was removed using the TURBO DNA-*free*™ Kit (Invitrogen #AM1907). RNA concentration was measured and equal amounts of RNA were used to synthesize cDNA with a reverse transcriptase kit (Qiagen). cDNA was amplified using primers targeting Adnp2 cryptic exon (339 bp, F: CTTGACAACATCAGGAAGGTGC, R: TTGTCCGGTATCTCGCTTTCT), Synjbp2 cryptic exon (224 bp, F: CTCCAACGACAGTGGCATCT, R: TCTTCCTGAGGACCTCCGTT), Usp15 cryptic exon (356 bp, F: GGTCCCTCTACTCCTAAGTCCC, R: TGGCTGTT CATTGTTTCTTCCAG), and Sort1-17B (350 bp, F: CAAATGCCAAGGTGGGATGAA, R: TTGAATCCAAAGCCTCTACGCC)[32,33]. PCR was performed using Phusion Plus green Master Mix (Thermo Scientific #F632L) with a modified touchdown PCR protocol. Products were visualized by agarose gel electrophoresis using SYBR safe.

Immunoblotting

Total protein was extracted from N2A cells using RIPA buffer (150 mM NaCl, 50mM Tris pH 7.4, 1% triton X-100, 0.1% SDS, 1% sodium deoxycholate) or from spinal cord tissue using lysis buffer (50mM Tris pH 7.5, 1mM EDTA, 150 mM NaCl, 1% SDS, 1% NP-40) with fresh protease inhibitors added. Protein samples were quantified using the BCA assay, separated using SDS-PAGE, transferred to nitrocellulose, and immunoblotted with antibodies against TDP-43 (Proteintech #10782-2-AP, 1:10,000), human-specific TDP-43 (Proteintech #60019-2-Ig, 1:10,000), GAPDH (Cell Signaling #5174, 1:3000) or TUJ1 (BioLegend #801202, 1:250). Secondary HRP-conjugated antibodies to appropriate species were added followed by detection with ECL Western blotting substrate (Pierce, USA).

Statistics

T-tests and ANOVA analysis were used to measure statistical significance (Prism, GraphPad). A p-value lower than 0.05 was considered significant.

Results

Stress granule assembly and disassembly *in vivo*

We have previously shown that mice bearing the TDP-43^{M337V} mutation have a robust defect in stress granule formation[16]. To determine if stress granule formation was similarly impaired in other TDP-43 mouse models expressing different mutations/levels of mutant protein, acute hyperthermia was applied to NEFH::rNLS8 mice which have doxycycline-inducible overexpression of cytoplasmic-restricted TDP-43 in neurons[30], and *Tardbp*^{Q331K} mice, which feature an ALS-causing mutation engineered into the mouse gene[20]. Both NEFH::rNLS8 and *Tardbp*^{Q331K} mice demonstrated normal stress granule formation (***Supplementary Fig. 1A-D***) and as anticipated levels of TDP-43 expression and localization (***Supplementary Fig. 1E-H***). Work from others suggests that both of these models do not reflect TDP-43 loss-of-function[20,34]. Consistent with this, neither model demonstrated the inclusion of TDP-43 repressed cryptic exons (*Adnp2*, *Synjbp2*, *Usp15*) or increased inclusion of *Sort1* alternate exon 17B (***Supplementary Fig. 1I, J***). Similarly, TDP-43^{M337V} mice, which express near-physiological levels of TDP-43^{M337V} protein owing to insertion of a single copy of human TDP-43^{M337V} genomic sequence into the mouse *Rosa26* locus[29], did not demonstrate robust inclusion of TDP-43-regulated cryptic exons, or alternative splicing of *Sort1*.

As the acute hyperthermia protocol is a terminal procedure[16], this precluded the evaluation of stress granule disassembly. Thus, we designed a new protocol in which awake, mildly restrained mice were maintained for 60 mins in an incubator set to 40˚C to induce stress granule formation in motor neurons (***Fig. 1A***). The internal body temperature of the mice was raised approximately 2.5˚C (39˚C avg internal temp) after 1 hr and normalized within 15 mins of their return to ambient temperature (***Fig. 1B***). Mice were continuously monitored throughout the 1 hr to ensure adequate respiration and absence of distress. After 1 hr, mice were given free access to food and water for the 15-min recovery period. Premised on our

prior work demonstrating that stress granules can be monitored in lumbar spinal cord neurons (L3-L5) by following the partitioning of cytoplasmic polyA mRNA (***Fig. 1C***), which is an obligate component of all stress granules, we established that this recurrent heat stress paradigm induced stress granule formation in ~50% of neurons at 60 mins, which fully disassembled after 15 mins of recovery (***Fig. 1D***). In addition to polyA mRNA and consistent with our previous work, the stress granule proteins TiaR, G3BP2, and HuR showed cytoplasmic demixing which also resolved after 15 mins of recovery (***Fig. 1C***), with HuR and G3BP2 showing colocalization (***Fig. 1E***). Note, we observed that not all protein markers were equivalent, with cytoplasmic TiaR puncta tending to persist after the 15 mins recovery period, while HuR and G3BP2 completely resolved (***Fig. 1D, arrows***). The variable protein patterns further validates the use of oligo-dT to track canonical stress granules. Overall, this revised heat stress paradigm facilitates the evaluation of both stress granule assembly and disassembly in mouse motor neurons *in vivo*.

Stress granule proteins, but not polyA mRNA, remain phase separated after recurrent hyperthermia

Consistent with our prior work using acute heat stress[16], motor neurons in TDP-43^{M337V} mice failed to form stress granules following 60 mins at 40˚C (***Supplementary Fig. 2***). Using mice aged 4 months (4M) and 12 months (12M), ages at which we have previously established that stress granule formation in motor neurons is intact *in vivo*[16], we performed two rounds of 60 mins stress followed by a 15 mins recovery period twice per week for four weeks in TDP-43^{M337V} transgenic mice and their non-transgenic (NTg) littermates (***Fig. 2A***). Over the course of the stress protocol, the average temperature increase per 60 mins session of hyperthermia was 1.8˚C and 3.0˚C in 4M and 12M animals, respectively (***Supplementary Fig. 3A, B***), and the weight of the mice remained stable (***Supplementary Fig. 3C, D***). After 4 weeks of recurrent heat stress, polyA mRNA granules were not detected in either 4M or 12M old mice of either genotype (***Fig. 2B***), as expected since stress granules are transient structures[35]. However, at both ages and in both genotypes, TiaR puncta were detected following recurrent stress exposure in a subset of lumbar spinal motor neurons (***Fig. 2C, insets***). In 4M NTg mice, TiaR puncta were observed in 66% of neurons in mice exposed to recurrent hyperthermia, in contrast to 37% of neurons in sham-treated animals (***Fig. 2D***). At 12M, NTg mice exposed to recurrent hyperthermia had significantly fewer neurons with TiaR puncta (30%). TDP-43^{M337V} mice largely mirrored NTg mice, with fewer neurons displaying

persistent TiaR puncta in 12M recurrently stressed animals compared to 4M mice (***Fig. 2E***). Given that stress granule formation is preserved in NTg, but impaired in TDP-43^{M337V} mice, this suggests that the formation of persistent TiaR puncta is independent of stress granule formation. Additionally, we observed persistent HuR and G3BP2 cytoplasmic puncta in NTg mice, suggesting a general persistence of stress granule proteins after recurrent hyperthermia, and that the persistence of TiaR puncta is not specific (***Supplementary Fig. 4***). TiaR is reported to also translocate to the cytoplasm following a stress exposure *in vitro*[36,37], thus we also quantified neurons with loss of nuclear TiaR after hyperthermia. Translocation of TiaR from the nucleus to the cytoplasm was significantly higher in stressed 4M NTg mice compared to sham-treated control mice, and was unchanged between conditions in 12M mice ***(Fig. 2F)***. In contrast, 4M and 12M TDP-43^{M337V} mice displayed a very small proportion of neurons with TiaR nuclear clearance (3-6%) and it was not stress-dependent (***Fig. 2G***). In summary, we report that stress granules, as labeled with polyA mRNA, resolve following recurrent hyperthermia, while cytoplasmic foci containing the RNA binding proteins TiaR, HuR, and G3BP2 do not. Further, we conclude that these persistent immunoreactive structures represent protein assemblies that are inconsistent with features of *bona fide* stress granules.

TDP-43^{M337V} mice develop neuronal cytoplasmic TDP-43 puncta in response to recurrent stress

It has been suggested that TDP-43 nuclear egress is part of a normal physiological response to stress[38–40]. Similar to what we have previously reported in a model of acute heat stress in this mouse model, TDP-43 nuclear clearance was observed in ~15% of the lumbar motor neurons of 4M NTg mice exposed to recurrent hyperthermia and was variable in 12M mice (***Fig. 3A, C)***. This stress-dependent relocalization of TDP-43 was absent in TDP-43^{M337V} mice exposed to recurrent hyperthermia and instead remained similar to sham-treated mice at both ages examined (***Fig. 3B, D***). To evaluate the presence of cytoplasmic TDP-43, we used two different commercial antibodies with reactivity to mouse and human TDP-43 (***Fig. 3E***). Specifically, a monoclonal antibody from R&D Biosystems (MAB7778) displayed larger cytoplasmic inclusions, while a polyclonal antibody available from Proteintech (10782-2-AP) showed several small cytoplasmic puncta within lumbar spinal neurons (***Fig. 3E***). Using the R&D Biosystems antibody for analysis, we detected TDP-43 puncta in ~35% of lumbar spinal neurons in 12M TDP-43^{M337V} mice exposed to recurrent hyperthermia, while they were

detected in only ~15% of neurons from age-matched NTg mice (***Fig. 3F***). Furthermore, it was evident that TDP-43 nuclear clearance and cytoplasmic puncta were almost completely independent events, with only 1.5% of neurons (6/400) showing co-occurrence of these events (***Fig. 3G***). Analysis of TDP-43 nuclear clearance and TDP-43 cytoplasmic puncta with the Proteintech antibody yielded similar results (***Supplementary Fig. 5***). To further assess TDP-43 pathology, we also labelled the motor cortex of 12M TDP-43^{M337V} mice with an aptamer that recognizes pathological TDP-43[41]. We observed that while both stressed mice and sham-treated controls have TDP-43 pathology, there was increased signal after hyperthermia (***Fig. 3H*).** As it is unclear whether the TDP-43 phenotypes we observed are associated with loss of TDP-43 function, we assessed the levels of three TDP-43 dependent cryptic exons in addition to splicing of *Sort1*, using N2A cells treated with TDP-43 siRNA as a positive control. Using RT-PCR of spinal cord lysates, no TDP-43 loss of function events were observed at baseline in TDP-43^{M337V} mice, nor with recurrent stress (***Fig. 3I***). Taken together, in response to recurrent stress, we observe cytoplasmic TDP-43 puncta in motor neurons, which are exacerbated by stress and genotype. Our data suggests that these changes are not associated with TDP-43 loss of function.

Neuronal TDP-43 cytoplasmic puncta are distinct from persistent TiaR puncta

A prevailing hypothesis in the ALS field is that persistent stress granules seed TDP-43 inclusions leading to motor neuron death[9]. Notably, we observed colocalization of TDP-43 cytoplasmic puncta with TDP-43 phosphorylated at S409/410, but no obvious overlap with the autophagy protein p62 (***Fig. 4A, B***)[42]. We leveraged our recurrent stress paradigm to directly evaluate whether cytoplasmic puncta of TDP-43 and TiaR are related. In both NTg and TDP-43^{M337V} mice, TDP-43 puncta and TiaR puncta were observed in different neurons, with only 5-12% of neurons displaying both TDP-43 and TiaR puncta (***Fig. 4C, D)***. Importantly, when TDP-43 puncta and TiaR puncta were detected in the same neuron, they were spatially distinct (***Fig. 4E, F***). Additionally, TDP-43 puncta did not overlap with the stress granule resident protein HuR (***Fig. 4E, F***). Our data indicate a clear distinction between cytoplasmic puncta that label for TDP-43 versus other RNA binding proteins using a recurrent heat stress paradigm *in vivo*.

Selective alpha motor neuron death in TDP-43^{M337V} mice following recurrent stress

We next examined whether heat-induced cytoplasmic TDP-43 or TiaR puncta, and nuclear TDP-43 clearance, were associated with motor neuron loss. To distinguish α- and γ-motor neurons, spinal cord sections were co-labelled for ChAT and NeuN. As has been reported[43], α-motor neurons express both ChAT and NeuN, whereas γ-motor neurons express ChAT, but not NeuN (***Fig. 5A, B)***. Following recurrent hyperthermia in 4M and 12M mice, total motor neuron counts (ChAT□) appeared comparable in NTg mice, while there was a neglible trend for stressed TDP-43^{M337V} animals to have less motor neurons than sham-treated controls (***Fig. 5C, D***). However, closer inspection of α- and γ-motor neurons revealed a significant 23% reduction in α-motor neurons exclusively in 12M hyperthermia-treated TDP-43^{M337V} mice compared to sham controls with no significant change in γ-motor neuron numbers between conditions (***Fig. 5E, F).*** There was no evidence of α- or γ-motor neuron loss in NTg mice at 4M or 12M (***Supplementary Fig. 6A, B***).

To determine whether these effects persisted after stress recovery, a separate cohort of 12M TDP-43^{M337V} and NTg mice were subjected to recurrent hyperthermia for 4 weeks followed by a 16 week recovery period (***Fig. 5G***). In this recovery paradigm, no persistent stress granules were observed at 20 weeks as assessed by polyA mRNA signal (***Supplementary Fig. 6C***). Additionally, neither cytoplasmic TiaR puncta, nor cytoplasmic TDP-43 puncta and nuclear clearance were detected in mice of either genotype (***Fig. 5H, Supplementary Fig. 6D***). At week 20, total motor neuron counts were reduced by 30% in TDP-43^{M337V} mice (***Fig. 5I***), driven entirely by a selective 42% loss of α-motor neurons (***Fig. 5J***), while γ-motor neurons remained unaffected (***Fig. 5K***). In contrast, motor neuron counts were unaffected by recurrent heat stress in NTg littermates, neither immediately after heat exposure (***Fig. 5B, Supplementary Fig. 6***) or following 16 weeks of recovery (***Fig. 5I***).

Taken together, these results indicate that recurrent hyperthermia induces cytoplasmic TiaR puncta that are reversible and not associated with motor neuron death, as they are detected in both NTg and TDP-43^{M337V} mice and resolve during recovery. However, in TDP-43^{M337V} mice, we note that a subset of neurons exhibiting cytoplasmic TDP-43 puncta (40%), which are not detectable after recovery, parallel a subset of neurons that are lost (44%). We infer that the neurons which were lost are the same neurons that displayed TDP-43 cytoplasmic puncta. Thus, recurrent hyperthermia in genetically predisposed mice reproduces key features

of ALS pathology, including nuclear TDP-43 clearance, cytoplasmic TDP-43 puncta formation, and selective vulnerability of α-motor neurons.

Discussion

The hypothesis that stress granules act as crucibles for TDP-43 inclusions, which trigger motor neuron death in ALS, is largely based on *in vitro* studies that rely on overexpression of aggregation-prone proteins[10,44,45]. Here, we employed a recurrent hyperthermia model and a mouse model expressing near-physiological levels of human mutant TDP-43 protein to probe this relationship *in vivo*. The homozygous TDP-43^{M337V} mouse model used in this study exhibits a 1.1x-fold expression of human TDP-43 compared to endogenous mouse Tdp-43. This model permits interrogation of the consequence of this disease-associated mutation, avoiding the pitfalls of gross overexpression. Using 60 mins hyperthermia exposure in awake, restrained mice, we observed stress granule formation and dissolution in lumbar motor neurons, as assessed by polyA mRNA and canonical stress granule protein markers. Extending the 60 mins stress to a recurrent paradigm allowed us to observe that while polyA mRNA-positive granules did not persist after 16 hyperthermia exposures delivered over the course of one month, puncta labelling for stress granule-resident proteins TiaR, G3BP2, and HuR did. Interestingly, young (4M) TDP-43^{M337V} mice displayed a similar frequency of TiaR puncta as NTg animals, despite their known stress granule assembly defect[16]. The concept that stress granule proteins can assemble into RNA-deficient aggregates is not novel[46]. For example, poliovirus-infected cells form Tia1 and TiaR positive aggregates that are distinct from stress granules, since they lack polyadenylated mRNA[46]. Notably, poliovirus induces cell death in part by suppressing the stress granule response[47]. This phenomenon loosely parallels our observations in TDP-43^{M337V} mice, which fail to form stress granules yet still exhibit TiaR-positive cytoplasmic puncta. Similar to stress granules, phase-separated TDP-43 is thought to be stabilized by RNA interactions that limit its cytoplasmic aggregation[48–50]. In our recurrent stress paradigm, the absence of polyadenylated mRNA puncta, together with positive staining using an aptamer that selectively recognizes RNA-deficient TDP-43[41], suggests that the TDP-43 puncta formed under these conditions more closely resemble aggregates than dynamic phase-separated assemblies. Importantly, hyperthermia-induced persistent TiaR puncta do not correlate with motor neuron loss, indicating that the persistence

of stress granule protein puncta is not inherently pathological as they are also observed in NTg animals that have no motor neuron loss.

In aged (12M) TDP-43^{M337V} mice exposed to recurrent hyperthermia, we observed both nuclear clearance of TDP-43 and cytoplasmic puncta formation, but strikingly, these events were mutually exclusive within individual neurons and independent of the formation of polyA mRNA-positive stress granules. Additionally, TDP-43 puncta were observed to be spatially distinct of TiaR or HuR puncta, which does not support a recent report, using overexpression of a cytoplasmic-restricted TDP-43 variant (TDP-43$^{\Delta NLS}$), claiming that stress granules scaffold TDP-43 phase separation[8,51]. We appreciate that our observations capture static endpoints after one month of stress, so we cannot exclude sequential or overlapping events during the recurrent hyperthermia paradigm. However, our data are consistent with other work that demonstrates that demixing of TDP-43 puncta from stress granules is associated with cell death and suggests that this separation is a key driver of the cell death phenotype[52].

Similar to many TDP-43 mouse models that have near physiological levels of TDP-43, TDP-43^{M337V} mice exhibit no motor neuron loss, as assessed up to 24M[29]. However, after recurrent hyperthermia, these mice developed selective alpha motor neuron loss, which worsened during a recovery period. Intriguingly, motor neuron loss was inversely correlated with TDP-43 puncta frequency. At 4M and 12M, translocation and puncta formation were observed without significant neuron loss but after a recovery period, motor neuron death was evident while TDP-43 localization was primarily nuclear in surviving neurons. This suggests that in this model, either TDP-43 nuclear clearance or puncta formation can trigger neurodegeneration, though we cannot yet distinguish their relative toxicity.

Reproducing the *genetics x time x environment* model of ALS

To integrate our findings within a broader framework, we refer to the model proposed by Al-Chalabi and Hardiman [17], which conceptualizes ALS as arising from the intersection of genetic susceptibility, aging, and environmental exposures. In our study, we modeled these components using aged TDP-43^{M337V} mice subjected to recurrent hypothermia exposures (***Fig. 7***). Unlike TDP-43 overexpression models with severe phenotypes[30,53], TDP-43 models with physiological expression show only mild FTD-like, but not motor, deficits[19,20]. Our findings here support the idea that these models require a “second hit” to unmask

neurodegenerative processes. In our system, aging provides a third factor, leading to a "three-hit" model where genetic predisposition, environmental stress, and time converge to elicit ALS-like pathology, similar to human ALS[17]. Consistent with prior *in vitro* observations[54], our data also suggest that nuclear TDP-43 clearance precedes cytoplasmic puncta formation in the context of ALS burden. Finally, it is important to note that this "three-hit" model which reproduces major features of ALS pathophysiology emerges in the context of defective stress granule assembly. We propose that this recurrent hyperthermia model can be leveraged to study early TDP-43-mediated disease mechanisms and to evaluate preclinical therapeutics targeting TDP-43 mislocalization or loss of function.

Conclusion

In this study, we leveraged a recurrent hyperthermia paradigm to demonstrate that persistent, stress-induced TiaR puncta are not toxic to spinal motor neurons in aged mice *in vivo* and do not spatially or temporally correlate with TDP-43 puncta following repeated stress. Consistent with this dissociation, we show that in the TDP-43^{M337V} mouse model where stress granule assembly is impaired, stress exposure nonetheless induces TDP-43 nuclear clearance and cytoplasmic puncta accumulation. This TDP-43 disease signature is accompanied by a progressive and selective loss of spinal α-motor neurons during cycles of stress and recovery. Importantly, the presence of motor neuron degeneration demonstrates that TDP-43 mislocalization, rather than the persistence of TiaR puncta, correlates with selective α-motor neuron vulnerability in the spinal cord. This is evidence that TDP-43 puncta arise independent of canonical stress granule proteins in a mouse model expressing physiologically relevant levels of TDP-43 and directly challenges the idea that stress granule inhibition is an effective therapeutic avenue. Lastly, the presented data indicate that the convergence of genetic susceptibility, environmental stress, and time is sufficient to drive both molecular and cellular hallmarks of neurodegenerative disease.

Data availability

The data that support the findings of this study are available from the corresponding author, upon reasonable request.

Acknowledgements

We thank all CVV lab members for helpful insights and discussion. We also thank Kevin Talbot for providing the TDP-43^{M337V} mice and Aurélie Cleret-Buhot from the CRCHUM imaging platform for technical support.

Funding

This project was funded by grants from CIHR and ALS Canada/Brain Canada (CVV). AD was supported by CIHR and ALS Canada Doctoral Awards, MC and MG were supported by ALS Canada Doctoral Awards, in collaboration with Brain Canada and Fondation Vincent-Bourque, respectively. AA received partial support from the Brain Canada Rising Stars Trainee program. CF was funded by an NSERC Undergraduate Research Award. JMG and HS were supported by NIH TR01 (1R01NS127186) to JMG employing HS, Target ALS Early-Stage ALS Clinician Fellowship (FS-2023-ESC-S2), and an MNDA Project Grant: Gregory/Oct25/2524-792.

Competing interests

The authors report no competing interests.'

Supplementary material

Supplementary material is available at *Brain* online.

References

1. Protter DSW, Parker R. Principles and Properties of Stress Granules. *Trends Cell Biol*. 2016;26(9):668-679.

2. Fujikawa D, Nakamura T, Yoshioka D, et al. Stress granule formation inhibits stress-induced apoptosis by selectively sequestering executioner caspases. *Curr Biol*. Published online April 21, 2023. doi:10.1016/j.cub.2023.04.012

3. Wheeler JR, Matheny T, Jain S, Abrisch R, Parker R. Distinct stages in stress granule assembly and disassembly. *Elife*. 2016;5. doi:10.7554/eLife.18413

4. Bravo-Jimenez MA, Sharma S, Karimi-Abdolrezaee S. The integrated stress response in neurodegenerative diseases. *Mol Neurodegener*. 2025;20(1):20.

5. Marlin E, Viu-Idocin C, Arrasate M, Aragón T. The Role and Therapeutic Potential of the Integrated Stress Response in Amyotrophic Lateral Sclerosis. *Int J Mol Sci*. 2022;23(14). doi:10.3390/ijms23147823

6. Liu-Yesucevitz L, Bilgutay A, Zhang YJ, et al. Tar DNA binding protein-43 (TDP-43) associates with stress granules: analysis of cultured cells and pathological brain tissue. *PLoS One*. 2010;5(10):e13250.

7. Mori F, Yasui H, Miki Y, et al. Colocalization of TDP-43 and stress granules at the early stage of TDP-43 aggregation in amyotrophic lateral sclerosis. *Brain Pathol*. 2024;34(2):e13215.

8. Yan X, Kuster D, Mohanty P, et al. Intra-condensate demixing of TDP-43 inside stress granules generates pathological aggregates. *Cell*. Published online May 15, 2025. doi:10.1016/j.cell.2025.04.039

9. Wolozin B, Ivanov P. Stress granules and neurodegeneration. *Nat Rev Neurosci*. Published online October 3, 2019. doi:10.1038/s41583-019-0222-5

10. Li YR, King OD, Shorter J, Gitler AD. Stress granules as crucibles of ALS pathogenesis. *J Cell Biol*. 2013;201(3):361-372.

11. Uechi H, Sridharan S, Nijssen J, et al. Small-molecule dissolution of stress granules by redox modulation benefits ALS models. *Nat Chem Biol*. Published online May 14, 2025:1-12.

12. Craig RA 2nd, De Vicente J, Estrada AA, et al. Discovery of DNL343: A Potent, Selective, and Brain-Penetrant eIF2B Activator Designed for the Treatment of Neurodegenerative Diseases. *J Med Chem*. 2024;67(7):5758-5782.

13. Flores BN, Yu SB, Cohen IV, et al. Investigational eIF2B activator DNL343 modulates the integrated stress response in preclinical models of TDP-43 pathology and individuals with ALS in a randomized clinical trial. *Nat Commun*. 2025;16(1):7690.

14. Koppenol R, Conceição A, Afonso IT, et al. The stress granule protein G3BP1 alleviates spinocerebellar ataxia-associated deficits. *Brain*. 2023;146(6):2346-2363.

15. Glineburg MR, Yildirim E, Gomez N, et al. Stress granule formation helps to mitigate neurodegeneration. *Nucleic Acids Res*. 2024;52(16):9745-9759.

16. Dubinski A, Gagné M, Peyrard S, Gordon D, Talbot K, Vande Velde C. Stress granule assembly in vivo is deficient in the CNS of mutant TDP-43 ALS mice. *Hum Mol Genet*. 2022;32(2):319-332.

17. Al-Chalabi A, Hardiman O. The epidemiology of ALS: a conspiracy of genes, environment and time. *Nat Rev Neurol*. 2013;9(11):617-628.

18. De Giorgio F, Maduro C, Fisher EMC, Acevedo-Arozena A. Transgenic and physiological mouse models give insights into different aspects of amyotrophic lateral sclerosis. *Dis Model Mech*. 2019;12(1). doi:10.1242/dmm.037424

19. Fisher EMC, Greensmith L, Malaspina A, et al. Opinion: more mouse models and more translation needed for ALS. *Mol Neurodegener*. 2023;18(1):30.

20. White MA, Kim E, Duffy A, et al. TDP-43 gains function due to perturbed autoregulation in a Tardbp knock-in mouse model of ALS-FTD. *Nat Neurosci*. 2018;21(4):552-563.

21. Dupuis L, Robertson J. Is amyotrophic lateral sclerosis less severe in mice than in humans? *Curr Opin Neurol*. Published online August 7, 2025. doi:10.1097/WCO.0000000000001412

22. Irwin KE, Jasin P, Braunstein KE, et al. A fluid biomarker reveals loss of TDP-43 splicing repression in presymptomatic ALS-FTD. *Nat Med*. Published online January 26, 2024. doi:10.1038/s41591-023-02788-5

23. Melamed Z, López-Erauskin J, Baughn MW, et al. Premature polyadenylation-mediated loss of stathmin-2 is a hallmark of TDP-43-dependent neurodegeneration. *Nat Neurosci*. Published online January 14, 2019. doi:10.1038/s41593-018-0293-z

24. Klim JR, Williams LA, Limone F, et al. ALS-implicated protein TDP-43 sustains levels of STMN2, a mediator of motor neuron growth and repair. *Nat Neurosci*. Published online January 14, 2019. doi:10.1038/s41593-018-0300-4

25. Ma XR, Prudencio M, Koike Y, et al. TDP-43 represses cryptic exon inclusion in the FTD-ALS gene UNC13A. *Nature*. 2022;603(7899):124-130.

26. Brown AL, Wilkins OG, Keuss MJ, et al. TDP-43 loss and ALS-risk SNPs drive mis-splicing and depletion of UNC13A. *Nature*. 2022;603(7899):131-137.

27. Armas JMB, Taoro-González L, Fisher EMC, Acevedo-Arozena A. Challenges of modelling TDP-43 pathology in mice. *Mamm Genome*. Published online April 29, 2025. doi:10.1007/s00335-025-10131-1

28. Kahriman A, Bouley J, Tuncali I, et al. Repeated mild traumatic brain injury triggers pathology in asymptomatic C9ORF72 transgenic mice. *Brain*. Published online August 1, 2023. doi:10.1093/brain/awad264

29. Gordon D, Dafinca R, Scaber J, et al. Single-copy expression of an amyotrophic lateral sclerosis-linked TDP-43 mutation (M337V) in BAC transgenic mice leads to altered stress granule dynamics and progressive motor dysfunction. *Neurobiology of Disease*. 2019;121:148-162. doi:10.1016/j.nbd.2018.09.024

30. Walker AK, Spiller KJ, Ge G, et al. Functional recovery in new mouse models of ALS/FTLD after clearance of pathological cytoplasmic TDP-43. *Acta Neuropathol*. 2015;130(5):643-660.

31. Martineau É, Di Polo A, Vande Velde C, Robitaille R. Dynamic neuromuscular remodeling precedes motor-unit loss in a mouse model of ALS. *Elife*. 2018;7. doi:10.7554/eLife.41973

32. Sinha IR, Sandal PS, Spence H, et al. Large-scale RNA-Seq mining reveals ciclopirox olamine induces TDP-43 cryptic exons. *Nat Commun*. 2025;16(1):6878.

33. Prudencio M, Jansen-West KR, Lee WC, et al. Misregulation of human sortilin splicing leads to the generation of a nonfunctional progranulin receptor. *Proc Natl Acad Sci U S A*. 2012;109(52):21510-21515.

34. Carmen-Orozco RP, Tsao W, Ye Y, et al. Elevated nuclear TDP-43 induces constitutive exon skipping. *Mol Neurodegener*. 2024;19(1):45.

35. Dormann D. The chains of stress recovery. *Science*. 2021;372(6549):1393-1395.

36. Rhine K, Li R, Kopalle HM, et al. Neuronal aging causes mislocalization of splicing proteins and unchecked cellular stress. *Nat Neurosci*. 2025;28(6):1174-1184.

37. Goswami B, Nag S, Ray PS. Fates and functions of RNA-binding proteins under stress. *Wiley Interdiscip Rev RNA*. 2023;15(1):e1825.

38. Huang WP, Ellis BCS, Hodgson RE, et al. Stress-induced TDP-43 nuclear condensation causes splicing loss of function and STMN2 depletion. *Cell Rep*. 2024;43(7):114421.

39. Zhang S, Vazquez-Sanchez S, Lu S, et al. Acetylation of lysine 82 initiates TDP-43 nuclear loss of function by disrupting its nuclear import. *bioRxiv*. Published online September 7, 2024:2024.09.04.611121. doi:10.1101/2024.09.04.611121

40. van Eersel J, Ke YD, Gladbach A, et al. Cytoplasmic accumulation and aggregation of TDP-43 upon proteasome inhibition in cultured neurons. *PLoS One*. 2011;6(7):e22850.

41. Spence H, Waldron FM, Saleeb RS, et al. RNA aptamer reveals nuclear TDP-43 pathology is an early aggregation event that coincides with STMN-2 cryptic splicing and precedes clinical manifestation in ALS. *Acta Neuropathol*. 2024;147(1):50.

42. Neumann M, Kwong LK, Lee EB, et al. Phosphorylation of S409/410 of TDP-43 is a consistent feature in all sporadic and familial forms of TDP-43 proteinopathies. *Acta Neuropathol*. 2009;117(2):137-149.

43. Tremblay E, Martineau É, Robitaille R. Opposite Synaptic Alterations at the Neuromuscular Junction in an ALS Mouse Model: When Motor Units Matter. *J Neurosci*. 2017;37(37):8901-8918.

44. Dewey CM, Cenik B, Sephton CF, Johnson BA, Herz J, Yu G. TDP-43 aggregation in neurodegeneration: are stress granules the key? *Brain Res*. 2012;1462:16-25.

45. Chen Y, Cohen TJ. Aggregation of the nucleic acid-binding protein TDP-43 occurs via distinct routes that are coordinated with stress granule formation. *J Biol Chem*. Published online January 10, 2019. doi:10.1074/jbc.RA118.006351

46. White JP, Lloyd RE. Poliovirus unlinks TIA1 aggregation and mRNA stress granule formation. *J Virol*. 2011;85(23):12442-12454.

47. White JP, Cardenas AM, Marissen WE, Lloyd RE. Inhibition of cytoplasmic mRNA stress granule formation by a viral proteinase. *Cell Host Microbe*. 2007;2(5):295-305.

48. Grese ZR, Bastos ACS, Mamede LD, French RL, Miller TM, Ayala YM. Specific RNA interactions promote TDP-43 multivalent phase separation and maintain liquid properties. *EMBO Rep*. 2021;n/a(n/a):e53632.

49. Duan L, Zaepfel BL, Aksenova V, et al. Nuclear RNA binding regulates TDP-43 nuclear localization and passive nuclear export. *bioRxiv*. Published online August 24, 2021:2021.08.24.457459. doi:10.1101/2021.08.24.457459

50. Mann JR, Gleixner AM, Mauna JC, et al. RNA Binding Antagonizes Neurotoxic Phase Transitions of TDP-43. *Neuron*. Published online February 27, 2019. doi:10.1016/j.neuron.2019.01.048

51. Mahendran TS, Wadsworth GM, Singh A, Gupta R, Banerjee PR. Homotypic RNA clustering accompanies a liquid-to-solid transition inside the core of multi-component biomolecular condensates. *Nat Chem*. 2025;17(8):1236-1246.

52. Gasset-Rosa F, Lu S, Yu H, et al. Cytoplasmic TDP-43 De-mixing Independent of Stress Granules Drives Inhibition of Nuclear Import, Loss of Nuclear TDP-43, and Cell Death. *Neuron*. Published online March 5, 2019. doi:10.1016/j.neuron.2019.02.038

53. Wils H, Kleinberger G, Janssens J, et al. TDP-43 transgenic mice develop spastic paralysis and neuronal inclusions characteristic of ALS and frontotemporal lobar degeneration. *Proc Natl Acad Sci U S A*. 2010;107(8):3858-3863.

54. Barmada SJ, Serio A, Arjun A, et al. Autophagy induction enhances TDP43 turnover and survival in neuronal ALS models. *Nat Chem Biol*. 2014;10(8):677-685.

Figure legends

Figure 1. Stress granules assemble and disassemble in vivo. (**A**) Schematic of stress paradigm with awake, restrained mice. Mice were perfused at T=0, T=60, and T=75 for analysis. (**B**) Temperature data for mice at T=0 (N=17), T=60 (N=17), and T=75 (N=9). Combined from NTg and TDP-43^{M337V} genotypes. Absolute temperature at each time point and increase during 60 min stress are presented. (**C**) Representative fluorescence *in situ*

hybridization (FISH) images for detection of polyadenylated mRNA in spinal motor neurons, and immunofluorescence (IF) images for stress granule resident proteins HuR, G3BP2, and TiaR. Scale bar 10 µm. Insets show granular signals for stress granule markers. Arrows show persistent TiaR puncta after 15 mins recovery (T=75). **(D)** Quantification of cells with stress granules at different time points using FISH images; T=0 (N=4), T=60 (N=6), T=75 (N=4). **(E)** Representative IF showing overlap of HuR and G3BP2 at 60 mins. Scale bar 10 µm.

Figure 2. **TiaR puncta, but not persistent stress granules, are present after recurrent hyperthermia. (A)** Schematic of stress paradigm for recurrent hyperthermia starting at 4M and 12M, performed in NTg and homozygous TDP-43^{M337V} mice. **(B)** Representative FISH images for polyA mRNA in spinal motor neurons at 4M and 12M. Scale bar 10 µm. **(C)** Representative TiaR images from spinal motor neurons at 4M and 12M. Scale bar 10 µm. Insets show persistent TiaR puncta in motor neurons after hyperthermia. **(D-E)** Quantification of neurons with TiaR puncta at 4M and 12M after stress; NTg: Control 4M (N=4), Stress 4M (N=4), Control 12M (N=3), Stress 12M (N=4); TDP-43^{M337V}: Control 4M (N=3), Stress 4M (N=6), Control 12M (N=5), Stress 12M (N=4). **(F-G)** Quantification of TiaR translocation in neurons at 4M and 12M. Cells were considered to have translocation when the nucleus showed no TiaR signal; NTg: Control 4M (N=4), Stress 4M (N=4), Control 12M (N=3), Stress 12M (N=4); TDP-43^{M337V}: Control 4M (N=5), Stress 4M (N=5), Control 12M (N=5), Stress 12M (N=4). One-way ANOVA was used to determine statistical significance.

Figure 3. TDP-43 translocation and puncta occur in motor neurons after recurrent hyperthermia. (A-B) Representative images of TDP-43 translocation and at 4M and 12M in NTg and TDP-43^{M337V} mice after recurrent stress. Scale bars are 10 µm. Yellow outlines depict neurons with TDP-43 nuclear clearance. **(C-D)** Quantification of cells with TDP-43 nuclear clearance at 4M and 12M. NTg: Control 4M (N=4), Stress 4M (N=4), Control 12M (N=3), Stress 12M (N=4); TDP-43^{M337V}: Control 4M (N=5), Stress 4M (N=5), Control 12M (N=5), Stress 12M (N=4). **(E)** Representative IF images TDP-43 cytoplasmic inclusions detected with two different antibodies (R&D Systems #MAB7778, Proteintech #10782-2-AP) after 12M recurrent stress. Yellow arrows point to TDP-43 puncta. Scale bars are 10 µm. **(F)** Quantification of neurons with TDP-43 puncta at 12M using R&D Biosystems antibody. NTg: Control 12M (N=5), Stress 12M (N=5), TDP-43^{M337V}: Control 12M (N=5), Stress 12M (N=4). **(G)** Analysis of relationship between TDP-43 nuclear clearance and puncta formation. NTg (N=119); TDP-43^{M337V} (N=111). **(H)** Representative images of labelling with TDP-43^{APT} to detect TDP-43 pathology in the motor cortex. TDP-43^{M337V} 12M Control N=2,

Stress N=2. **(I)** RT-PCR depicting cryptic *Adnp2*, cryptic *Synjbp2*, cryptic *Usp15*, and Sort1 exon17B in NTg and TDP-43^{M337V} mice following recurrent stress.

Figure 4. TDP-43 puncta resemble pathological inclusions and are independent of stress granule proteins. (A) Representative images showing overlap between TDP-43 inclusionswith Phospho-TDP-43 (Ser 409/410) in 12M TDP-43^{M337V} mice after recurrent stress. Scale bar 20 µm (Example 1), 10 µm (Example 2). **(B)** Representative image of p62 and TDP-43 in 12M TDP-43^{M337V} mice after recurrent stress. Scale bar 5 µm. **(C)** Representative images with neurons after recurrent stress exhibiting either TDP-43 (green) or TiaR (red) puncta. Scale bar 10 µm. **(D)** Analysis of relationship between TDP-43 puncta formation and TiaR puncta formation. NTg (N=111); TDP-43^{M337V} (N=111). **(E)** Representative images with neurons containing stress granule protein puncta (TiaR, HuR) that do not overlap with TDP-43 puncta. **(F)** Line scans showing partitioning of green (TDP-43) and red (SG protein) signals in zoomed images.

Figure 5. Selective, stress-induced, progressive motor neuron loss in TDP-43^{M337V} mice after hyperthermia. (A) Cartoon showing difference between alpha (α) and gamma (γ) motor neurons **(B)** Representative image of the ventral horn of a spinal cord to differentiate alpha and gamma motor neurons. Alpha (α) motor neurons are indicated with a hashtag (#) and gamma (γ) motor neurons are indicated with a star (*). Scale bar 50 µm. Total motor neuron counts in NTg **(C)** and TDP-43^{M337V} **(D)** mice at 4M and 12M following recurrent stress. **(E-F)** α and γ motor neuron counts in TDP-43^{M337V} mice at 4M and 12M. **(G)** Diagram of the stress and recovery paradigm used in 12M animals. **(H)** Representative picutres of TDP-43 and TiaR following a recovery period in 12M TDP-43^{M337V} mice. Scale bars 10 µm. Quantification of total **(I),** alpha **(J),** and gamma **(K)** motor neurons following a recovery period in NTg and TDP-43^{M337V} mice. For all graphs, each point represents a single mouse. One-way ANOVA analysis was used to determine statistical significance.

Figure 6. A model recapitulating the genes, time, environment hypothesis for ALS. (A) Model showing the genes, time, environment hypothesis in the context of this study using recurrent stress on 12M TDP-43^{M337V} mice. **(B)** Graph depicting the relationship between TiaR puncta, TDP-43 nuclear clearance, TDP-43 puncta, and motor neuron survival with increasing ALS burden.

FIGURE 1

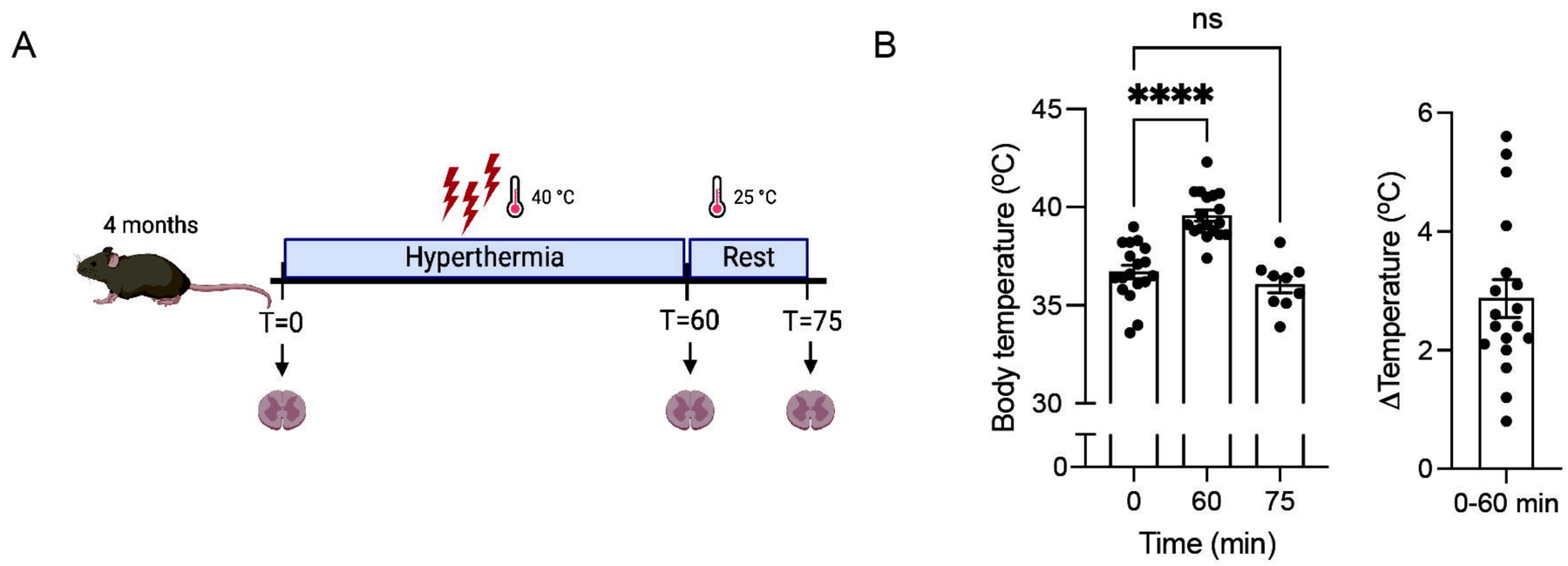
A
4 months
40 °C
25 °C
Hyperthermia
Rest
T=0
T=60
T=75
B
ns
****
Body temperature (ºC)
45
40
35
30
0
0
60
75
Time (min)
ΔTemperature (ºC)
6
4
2
0
0-60 min

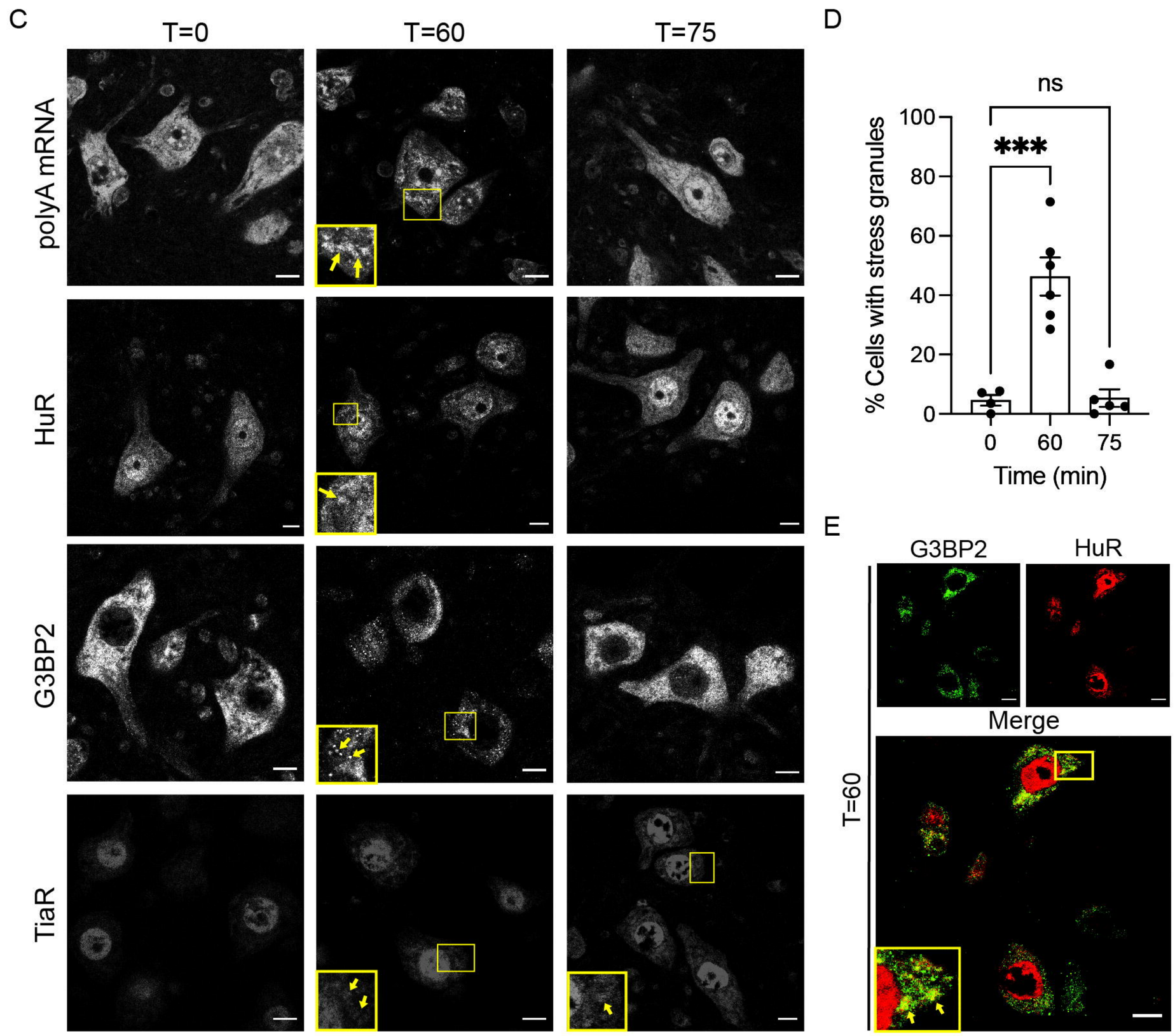
C
T=0
T=60
T=75
polyA mRNA
HuR
G3BP2
TiaR
D
ns
***
% Cells with stress granules
100
80
60
40
20
0
0
60
75
Time (min)
E
G3BP2
HuR
Merge
T=60

FIGURE 2

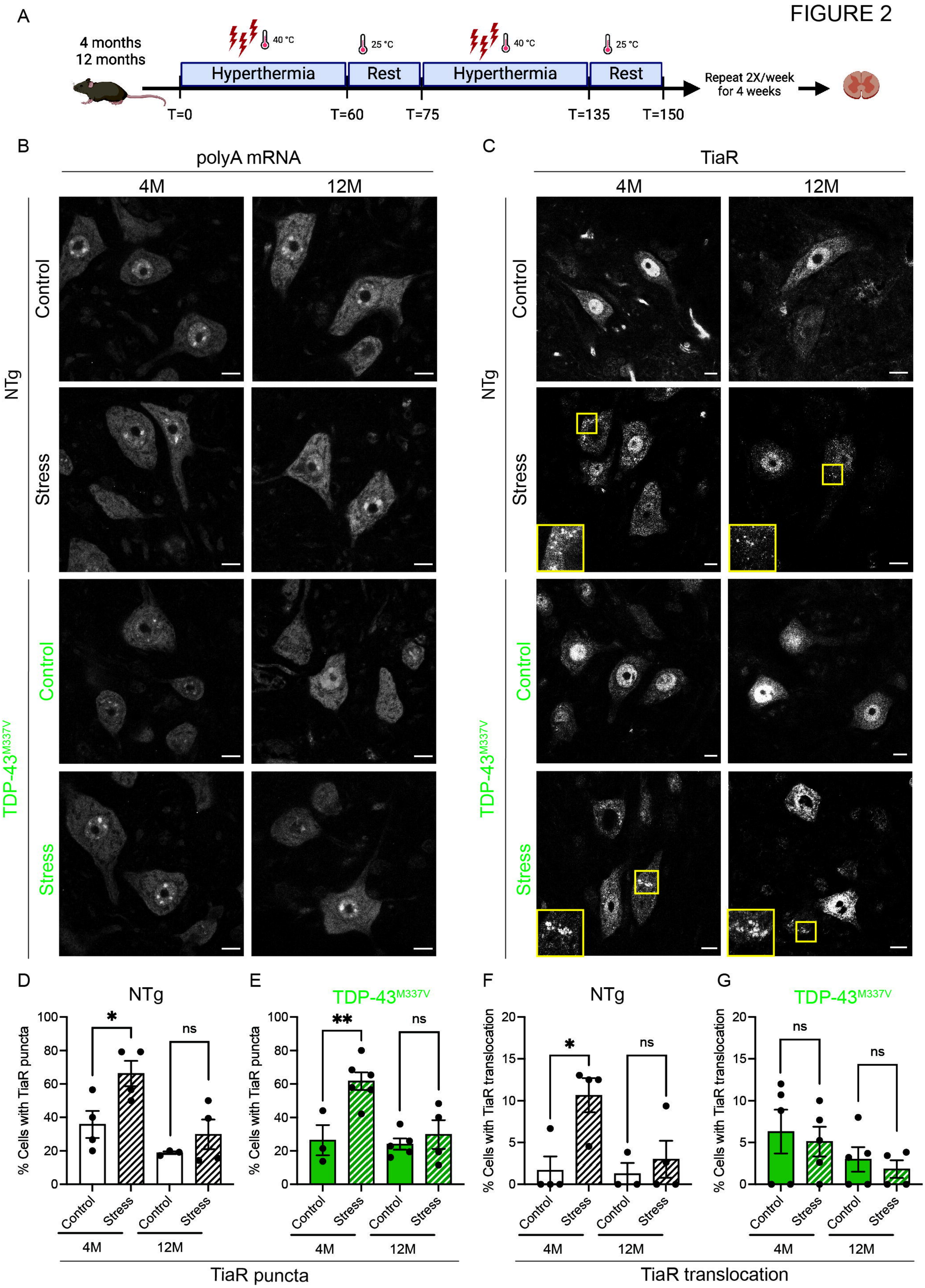
A
4 months
12 months
40 °C
25 °C
40 °C
25 °C
Hyperthermia
Rest
Hyperthermia
Rest
Repeat 2X/week
for 4 weeks
T=0
T=60
T=75
T=135
T=150
B
polyA mRNA
4M
12M
NTg
TDP-43M337V
Control
Stress
C
TiaR
D
NTg
% Cells with TiaR puncta
E
TDP-43M337V
TiaR puncta
F
% Cells with TiaR translocation
G
TiaR translocation
ns
*
**

FIGURE 3

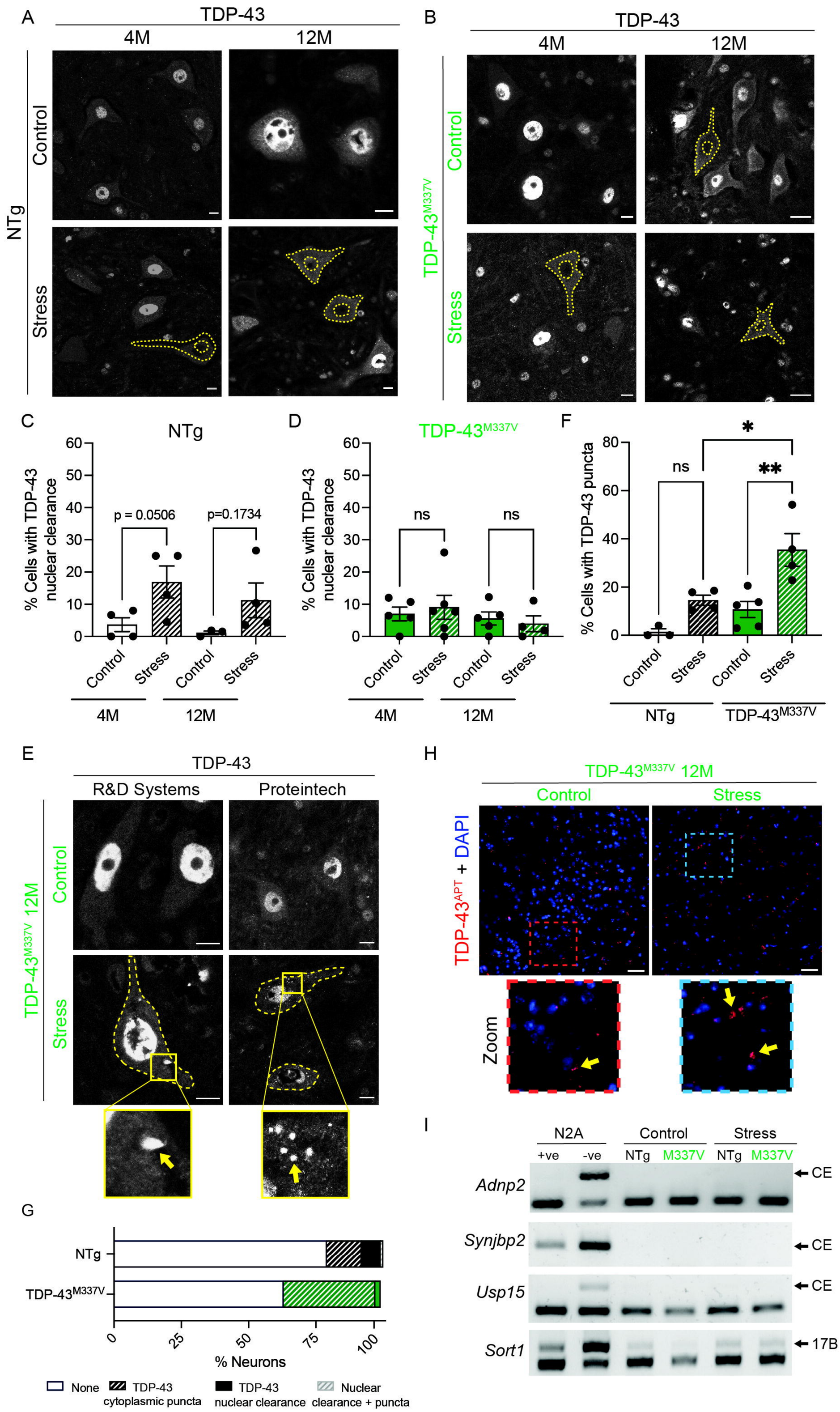
A
TDP-43
4M
12M
NTg
Control
Stress
B
TDP-43
4M
12M
TDP-43M337V
Control
Stress
C
NTg
% Cells with TDP-43 nuclear clearance
p = 0.0506
p=0.1734
Control
Stress
Control
Stress
4M
12M
D
TDP-43M337V
% Cells with TDP-43 nuclear clearance
ns
ns
Control
Stress
Control
Stress
4M
12M
F
% Cells with TDP-43 puncta
ns
*
**
Control
Stress
Control
Stress
NTg
TDP-43M337V
E
TDP-43
R&D Systems
Proteintech
TDP-43M337V 12M
Control
Stress
H
TDP-43M337V 12M
Control
Stress
TDP-43APT + DAPI
Zoom
G
NTg
TDP-43M337V
% Neurons
None
TDP-43 cytoplasmic puncta
TDP-43 nuclear clearance
Nuclear clearance + puncta
I
N2A
Control
Stress
+ve
-ve
NTg
M337V
NTg
M337V
Adnp2
Synjbp2
Usp15
Sort1
CE
CE
CE
17B

FIGURE 4

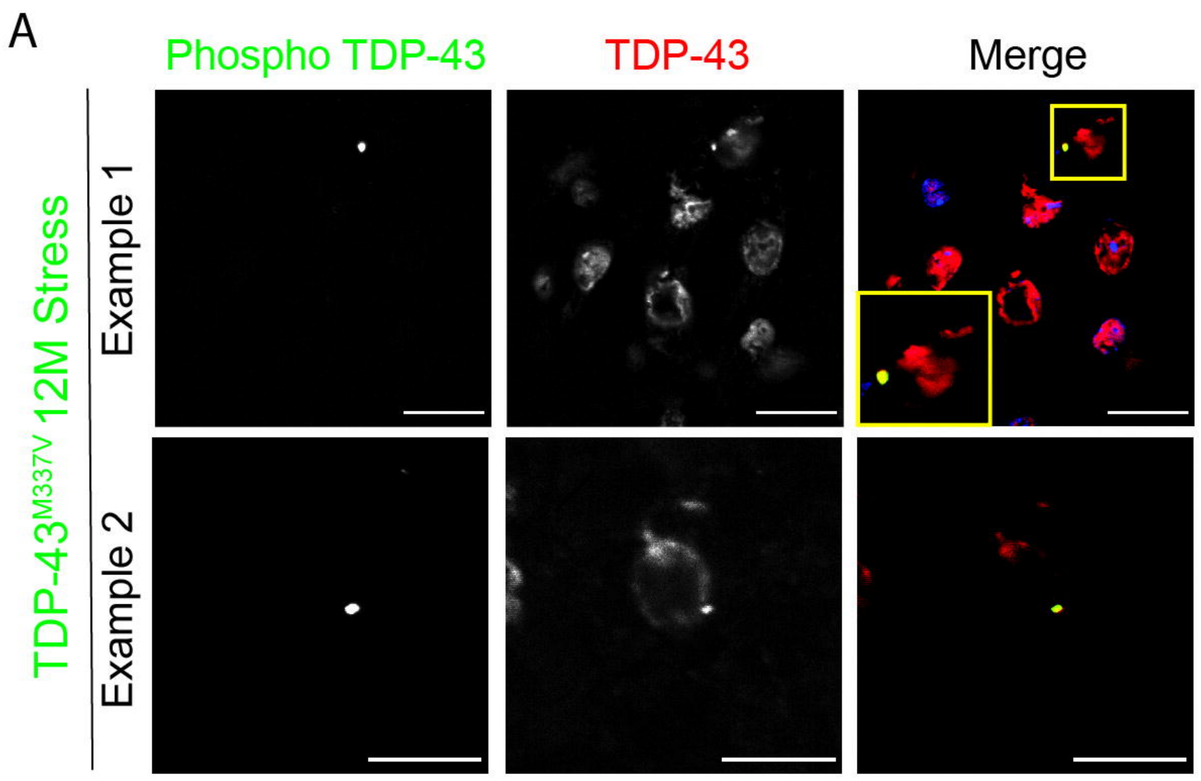
A
Phospho TDP-43
TDP-43
Merge
TDP-43M337V 12M Stress
Example 1
Example 2

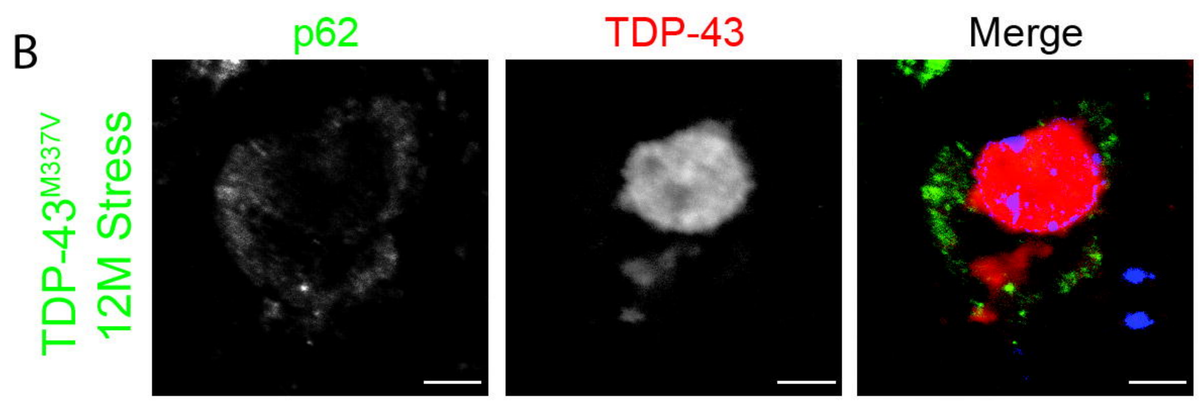
B
p62
TDP-43
Merge
TDP-43M337V 12M Stress

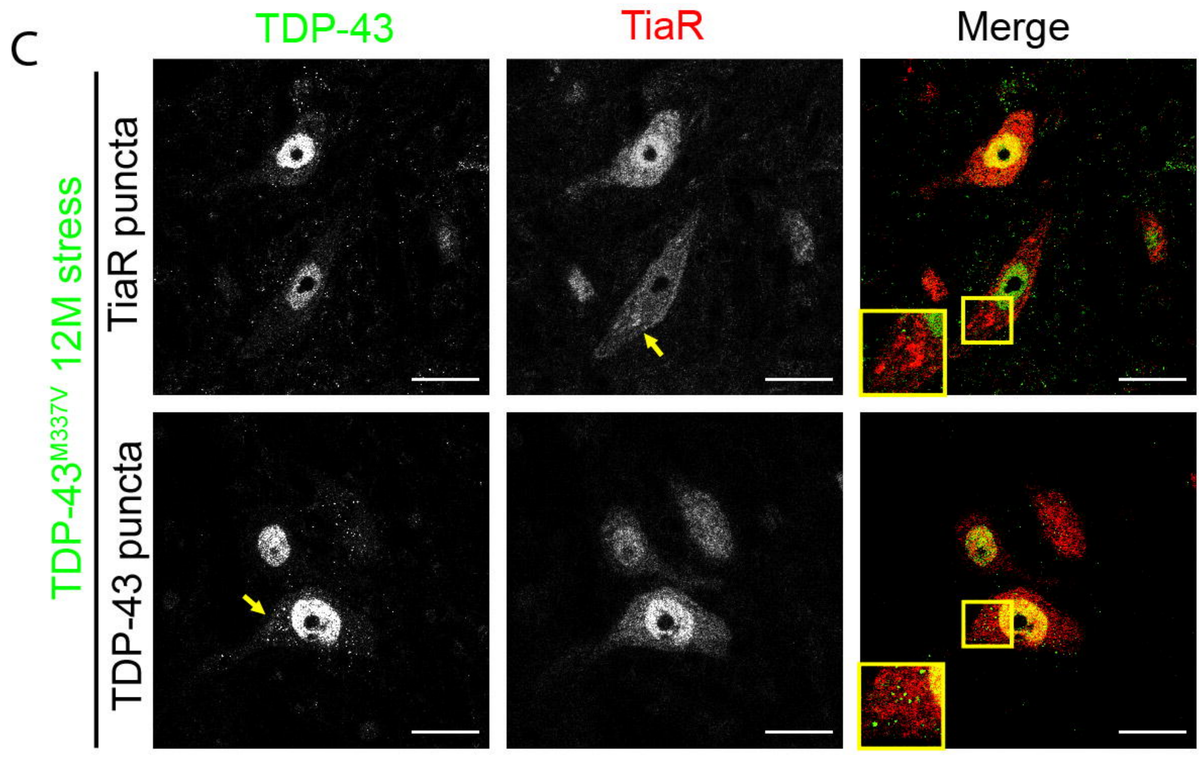
C
TDP-43
TiaR
Merge
TDP-43M337V 12M stress
TiaR puncta
TDP-43 puncta

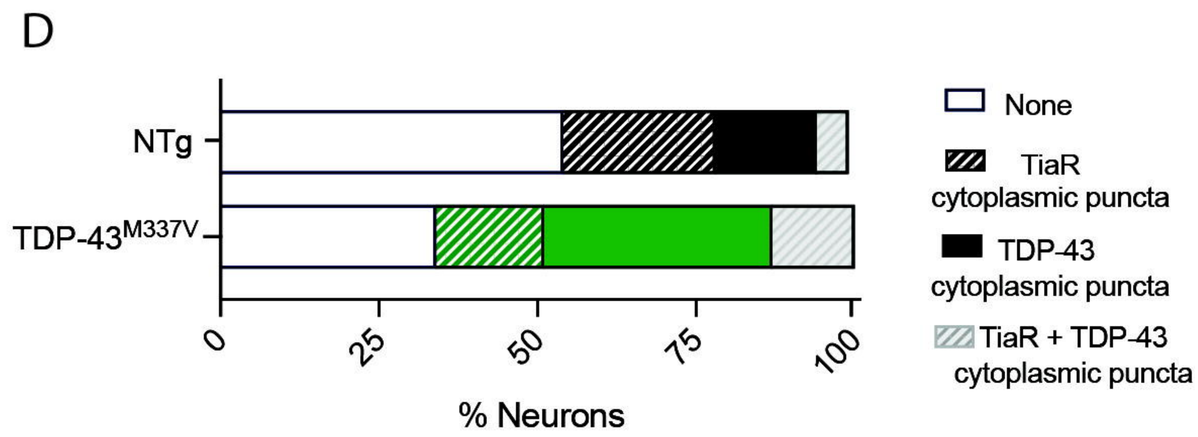
D
NTg
TDP-43M337V
0
25
50
75
100
% Neurons
None
TiaR cytoplasmic puncta
TDP-43 cytoplasmic puncta
TiaR + TDP-43 cytoplasmic puncta

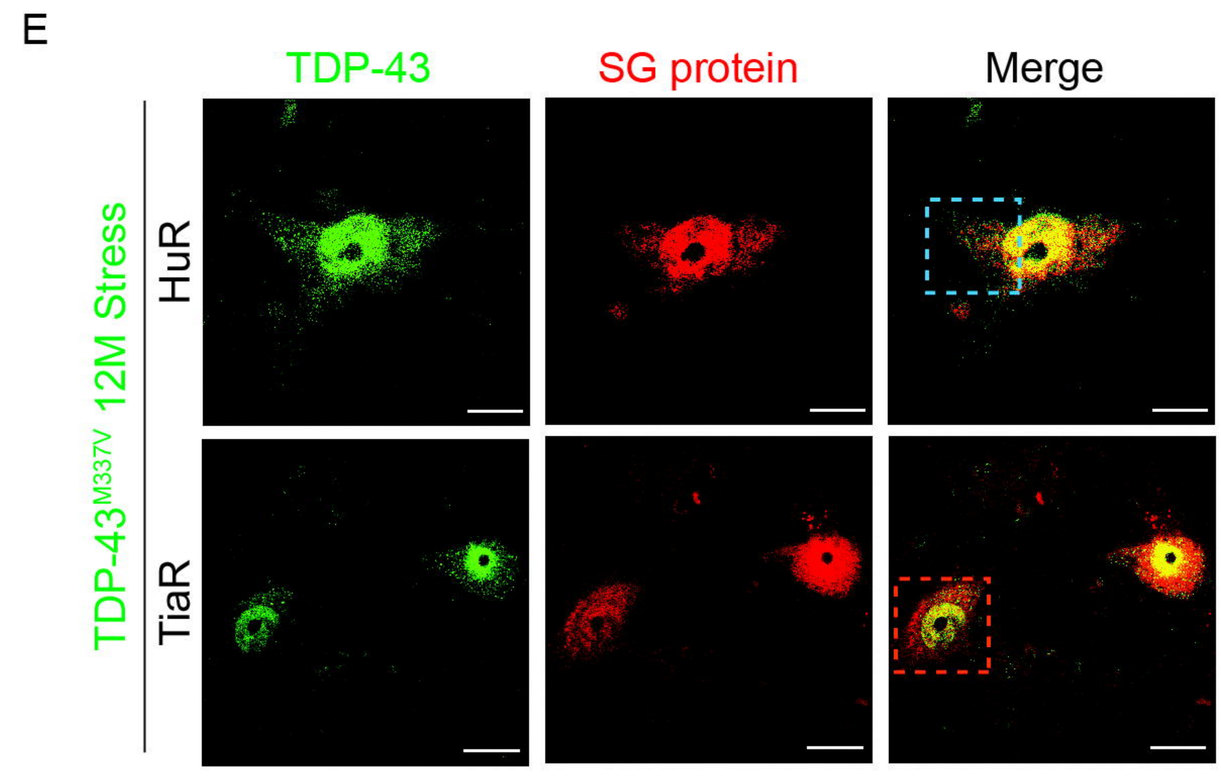
E
TDP-43
SG protein
Merge
TDP-43M337V 12M Stress
HuR
TiaR

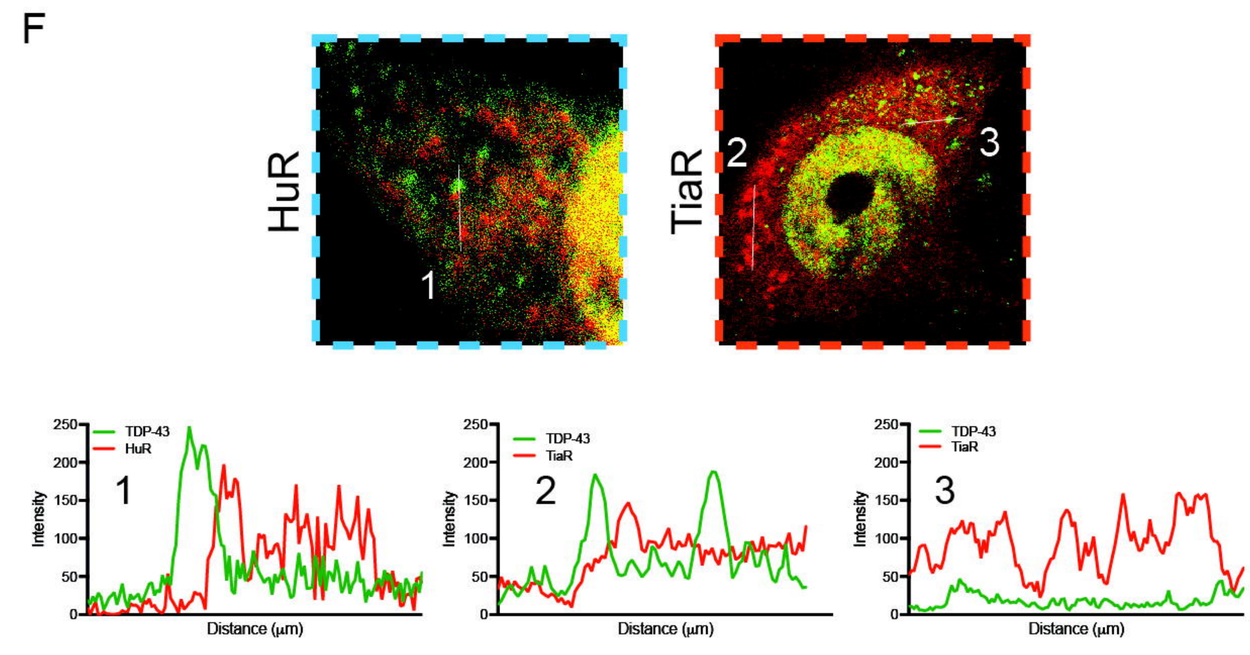
F
HuR
TiaR
1
2
3
TDP-43
HuR
TiaR
Intensity
Distance (µm)

FIGURE 5

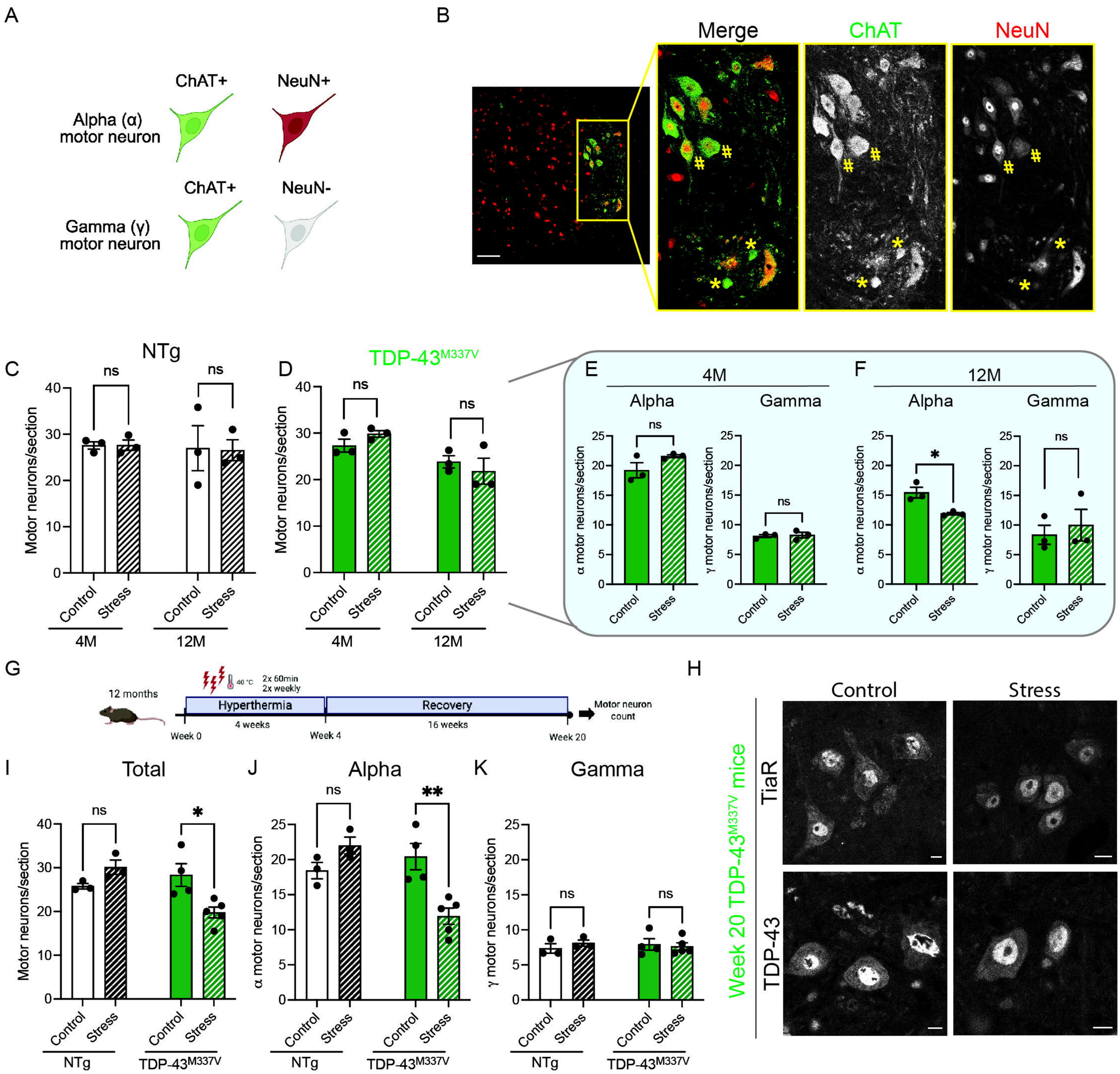
A
ChAT+
NeuN+
Alpha (α) motor neuron
ChAT+
NeuN-
Gamma (γ) motor neuron
B
Merge
ChAT
NeuN
C
NTg
ns
ns
Motor neurons/section
Control
Stress
4M
12M
D
TDP-43M337V
ns
ns
Motor neurons/section
Control
Stress
4M
12M
E
4M
Alpha
Gamma
ns
ns
α motor neurons/section
γ motor neurons/section
Control
Stress
F
12M
Alpha
Gamma
*
ns
α motor neurons/section
γ motor neurons/section
Control
Stress
G
12 months
40 °C
2x 60min
2x weekly
Hyperthermia
4 weeks
Recovery
16 weeks
Motor neuron count
Week 0
Week 4
Week 20
H
Control
Stress
TiaR
TDP-43
Week 20 TDP-43M337V mice
I
Total
ns
*
Motor neurons/section
Control
Stress
NTg
TDP-43M337V
J
Alpha
ns
**
α motor neurons/section
Control
Stress
NTg
TDP-43M337V
K
Gamma
ns
ns
γ motor neurons/section
Control
Stress
NTg
TDP-43M337V

FIGURE 6

A

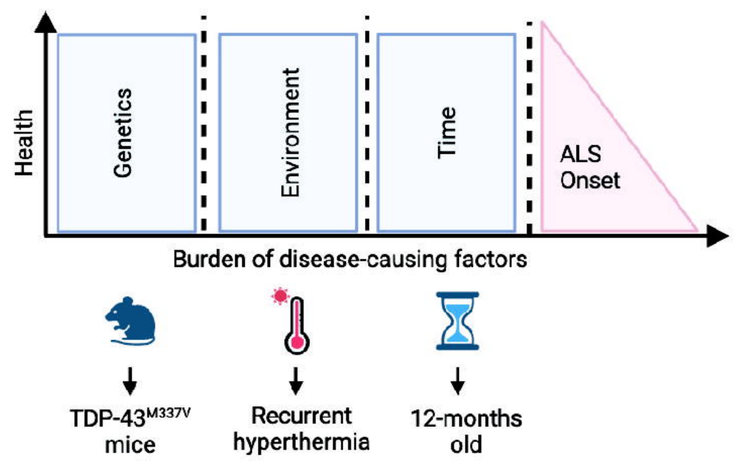

	Risk factors	Combination
None	0	None
Low	1	
Medium	2	
High	3	
Extreme	3 + time	+
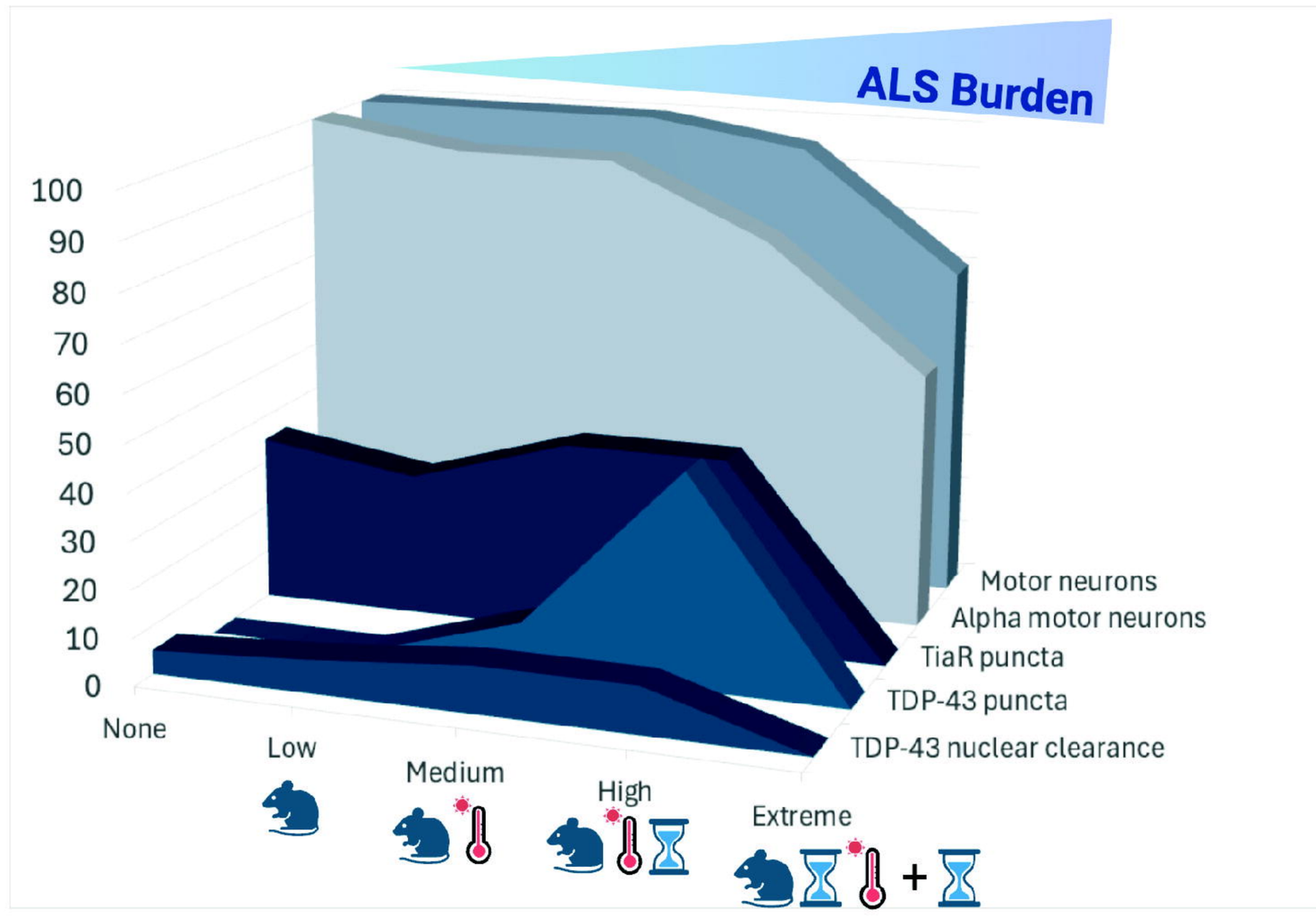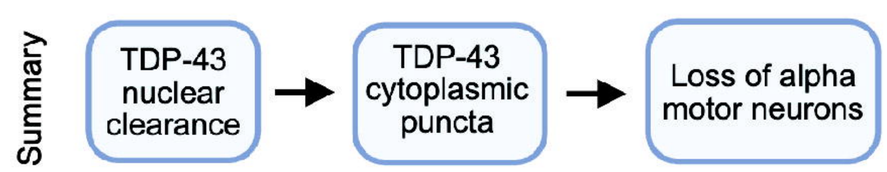
B